# Sea-Urchin-like Cobalt Oxide Grown on Nickel Foam as a Carbon-Free Electrode for Lithium−Oxygen Batteries

Xiujing Lin, Yesheng Shang, Liangyu Li, and Aishui Yu*

Department of Chemistry, Shanghai Key Laboratory of Molecular Catalysis and Innovative Materials, Institute of New Energy, Collaborative Innovation Center of Chemistry for Energy Materials, Fudan University, 2205 Songhu Road, Shanghai 200438, China

ABSTRACT: Rechargeable lithium−oxygen batteries have attracted extensive attention for their high energy density. However, the carbon corrosion, the undesired electrolyte decomposition catalyzed by carbon, and the irreversible reaction between carbon and the discharge product Li_2O_2 limit their performance. Herein we show the synthesis of sea-urchin-like cobalt oxide growing directly on nickel foam by a facile method, exhibiting several features. First, the open structure facilitates electrolyte penetration and the ion/electron transfer. Furthermore, the macrosized voids built up by the 1D nanorods provide sufficient buffer space for Li_2O_2 deposition without blocking O_2 diffusion. As a result, the battery displays high performance, including a high specific capacity of ∼3000 mAh g^{-1} based on the weight of the whole electrode and long-life (∼1800 h, 60 cycles at a fixed capacity of 500 mAh g^{-1}).

KEYWORDS: Lithium−oxygen batteries, Carbon-free, Sea-urchin-like cobalt oxide
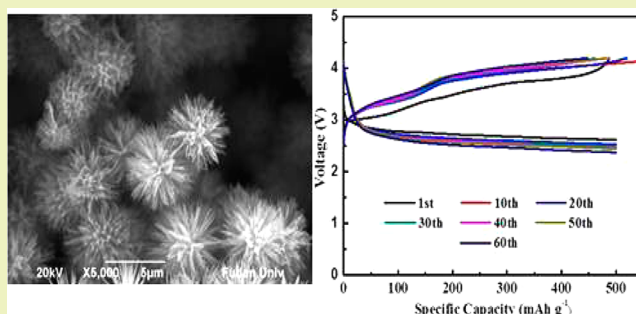
INTRODUCTION

The rechargeable lithium−oxygen batteries (Li−O_2) have recently attracted worldwide attention due to their highest energy density among the state-of-the-art batteries.[1,2] However, the practical applications of lithium−oxygen batteries still face substantial challenges, including large polarization, low round-trip efficiency, poor cyclability, and so on.

In an aprotic electrolyte, the fundamental electrode reaction is thought to be based on the reversible reaction of $2Li + O_2 \rightarrow Li_2O_2$. Upon discharge, Li^+ reduces molecular O_2 to form insoluble lithium peroxide, which continuously accumulates on the pores of the electrode and gradually blocks the electrolyte and oxygen pathways.[3−5] A desirable electrode must meet two essential prerequisites: (1) a large surface area to offer enough active sites for both the ORR and OER; (2) a large pore volume to store the discharge product. In this respect, carbon and carbon based materials are ideal candidates for porous electrodes, which have been revealed to exhibit electrochemical reactivity for ORR process.[4−12] However, recent reports have indicated the existence of carbon promotes the electrolyte decomposition, which is accelerated by the addition of metal catalysts.[13−15] In particular, the inevitable reaction between the discharge product Li_2O_2 and carbon occurs, leading to the formation of a single molecular layer of Li_2CO_3 at the carbon/Li_2O_2 interface.[16,17] Li_2CO_3 and other byproducts formed on the carbon surface cannot be completely decomposed and will accumulate on the active sites of carbon. As a consequence, carbon-based electrode exhibits much higher charge potentials than the equilibrium value, which induce the large voltage gap and decaying cycling performance.

A possible solution to the problems mentioned above is to design a carbon-free air electrode with open frameworks for Li_2O_2 deposition.[18] The replacement of carbon with nanoporous gold foil and Ru/ITO as the air electrode in the lithium−oxygen battery was attempted respectively and thus showed reduced overpotentials and excellent cycling stability.[19−21] Here, we report a carbon-free electrode design based on cobalt oxide, which was prepared by a facile method, to relieve the carbon-induced problems in lithium−oxygen batteries. Co_3O_4 has been demonstrated to act as an active catalyst for both oxygen reduction (ORR) and oxygen reduction reaction (OER).[22−24] The as-synthesized electrode possess many vital factors, including open structure for electron/ion transfer, optimized porous structure to provide efficient buffer space for discharge product deposition/decomposition. As a result, the battery exhibits high capacity and long-life.

EXPERIMENTAL SECTION

Preparation of Co_3O_4@Ni Electrode. The sea-urchin-like Co_3O_4 microspheres were synthesized on nickel foam by a hydrothermal method. The Ni foam current collector was pretreated by degreasing with acetone, etching with 6.0 mol dm^{-3} HCl for 15 min, and then rinsing with deionized water extensively. In detail, 0.4362 g of $Co(NO_3)_2$·$6H_2O$ and 0.42 g of urea were first dissolved in 30 mL of deionized water. The solution was kept stirring for 15 min and then transferred into a 50 cm^3 Teflon-lined stainless steel autoclave. The
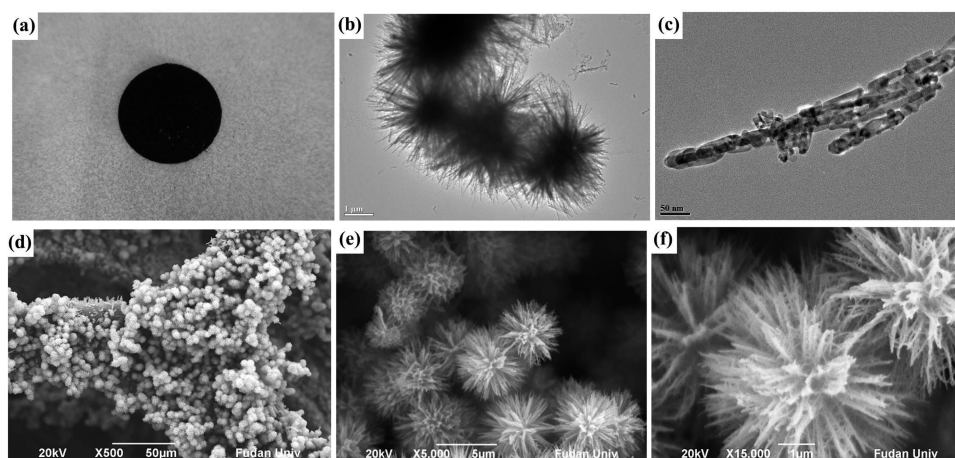
Figure 1. (a) Photo, (b, c) TEM images, and (d, e, f) SEM images of the Co_3O_4@Ni electrode.

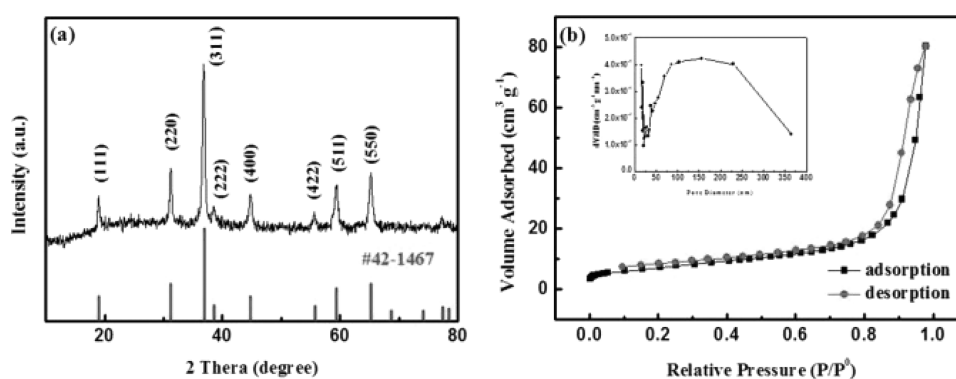**Figure 2.** (a) XRD patterns and (b) nitrogen adsorption/desorption isotherm. Inset in panel b is the pore-size distribution of the Co_3O_4@Ni electrode.

treated nickel foam was immersed in the reaction solution for 8 h at 95 °C to allow the growth of precursor. After that, the autoclave was cooled down to room temperature naturally and the nickel foam was removed from the growth solution, thoroughly washed with water, dried at 60 °C, and finally calcined at 400 °C for 3 h in air. On average, 2−3 mg nanowires were grown on a per cm^2 nickel foam.

Physical Characterization. The morphologies of free-standing Co_3O_4@Ni electrode were observed by scanning electron microscopy (SEM, JEOL JSM-6390) and transmission electron microscopy (TEM, JEM-2100F). The structure of the as-prepared material was characterized by a Bruker D8 Advance X-ray diffractometer using Cu Kα radiation at a scan rate of 5° min^{-1}. N_2 adsorption/desorption isotherms were obtained using a Micromeritics Tristar 3000. Fourier-transform infrared reflection (FTIR) measurements were carried out on a Shimadz IRPrestige-21 FTIR spectrometer using KBr pellet. The impedance variation was monitored by electrochemical impedance spectroscopy (EIS) in the frequency range of 0.01 to 10^5 Hz with an amplitude of 5 mV.

Electrochemical measurement. The as-synthesized Co_3O_4@Ni was pressed and directly utilized as the air electrode for lithium−oxygen batteries without any additional treatment. For charge/discharge tests, lithium−oxygen batteries were constructed in an argon atmosphere glovebox ($H_2O \leq 10$ ppm) using Swagelok batteries with an air window of 78.5 mm^2. They were assembled by stacking a Li foil, a Celgard 3500 membrane and Co_3O_4@Ni electrodes. The nonaqueous electrolyte consisted of 0.5 M lithium bis-(trifluoromethanesolphonyl)imide (LiTFSI) in tetraethylene glycol dimethoxyethane (TEGDME). Charge/discharge measurements were performed on a Land cycler (Wuhan Jinnuo Electronic Co. Ltd.) in the voltage range of 2.0−4.2 V vs Li^+/Li at various discharge current densities in a pure/dry oxygen-filled glovebox. All of the tests were performed at room temperature.

RESULTS AND DISCUSSION

The nickel foam was first punched into small disks with a diameter of 12 mm and then put into a Teflon reactor. After the growth and calcination processes, a visible black coating in the whole nickel foam is clearly observed (Figure 1a). The XRD analysis is carried out for the structure identification and the results reveal that Co_3O_4, which was scratched from the nickel foam, can be obtained by calcining the as-deposited material (Figure 2a). The morphology and structure of the Co_3O_4@Ni electrode is observed by SEM. As shown in Figure 1d−f, a representative overview of the sea-urchin-like microspheres around 5 um in diameter is displayed. The higher magnification SEM image in Figure 1f shows that individual sea-urchin-like Co_3O_4 microsphere packs with numerous densely 1D nano-rods, which evenly spread out along radial direction and the length is about 1−2 um. The results of TEM are consistent with the SEM results, indicating that the synthesized sea-urchin-like structure is composed of individually aligned 1D nanorods that are tightly bundled perpendicularly to a central core. The HRTEM image of a few 1D nanostructures (Figure 1c) shows that they are composed of interconnected nanorods. This unique structure enables the surface of nanorods highly accessible to the reactants and also provides enough void volume for the discharge product deposition.

The pore size and specific surface area of Co_3O_4 were characterized by N_2 adsorption/desorption isotherms measurements. As shown in Figure 2b, the observed isotherm of the prepared is a typical type IV adsorption with a surface area of

25.5 m^2 g^{-1} and a hysteresis loop in the P/P_0 range of 0.9−1.0 is observed, indicating the presence of macropores. The pore size distribution curve shows that the prepared Co$_3$O$_4$ exhibits broad pore size distributions. The unique mesoporous/macroporous hierarchical structure can effectively provide disorder-free channels of oxygen vacancies, and thereby improve the electrocatalytic performance.[25]

Cyclic voltammetry (CV) was employed to investigate the catalytic activity of the Co$_3$O$_4$@Ni electrode. As presented in Figure 3, the CV curve in argon shows no obvious cathodic or

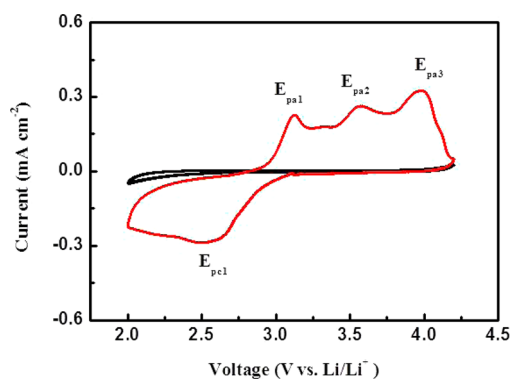**Figure 3.** Cyclic voltammetry curves of Co$_3$O$_4$@Ni electrode in the electrolyte containing 0.5 M LiTFSI/TEGDME under O$_2$ atmosphere at a scan rate of 0.1 mV s^{-1}.

anodic peak current, indicating its stability in the electrolyte in the voltage range of 2.0−4.2 V. When performed in O$_2$ atmosphere, obvious ORR and OER peaks were observed, demonstrating promising catalytic activity toward both ORR and OER processes. According to the literature by K. M. Abraham,[26] the broad reduction peaks at ∼2.60 V indicate that more than one reduction reaction occurs, which could be assigned to the formation of O$_2^-$, O$_2^{2-}$, and O^{2-}. Three overlapping anodic peaks result from the single cathodic peak, suggesting the oxidation of the products formed from the reduction at E$_{pc1}$.

The Co$_3$O$_4$@Ni was used as the air electrode for rechargeable lithium−oxygen batteries without any additional treatment. To exclude possible electrochemical contributions from the substrate, the pure Ni foam was used as the air electrode and discharged to 2.0 V in O$_2$ at a current density of 0.05 mA cm^{-2}. The discharge profile of the Ni foam presented in Figure 4 terminated in a substantially short time (∼26 s), without discharge plateau, while the Co$_3$O$_4$@Ni electrode discharged for several days (∼72 h). Thus, Ni foam is proved to make no contributions to the discharge capacity when used as the substrate and current collector. Figure 5a displays the first charge/discharge profile of the Co$_3$O$_4$@Ni-based battery at a current density of 0.05 mA cm^{-2}. A specific capacity of 3035 mAh g^{-1} with comparable charge capacity could be achieved. The discharge potential shows an average value of ca. 2.61 V vs Li/Li$^+$ and then decays gradually down to 2.0 V. An apparent three-stage process is recorded during the charge process, which could be ascribed to the electrochemical oxidation of the outer part of Li$_2$O$_2$ particles (stage I), the electrochemical oxidation of the bulk Li$_2$O$_2$ particles (stage II), and the undesired decomposition of the electrolyte (stage III).[27] It should be noted that the Co$_3$O$_4$@Ni electrode also exhibits considerably low charge voltage for the OER process at ca. 3.85 V vs Li/Li$^+$, substantially lower than that of other reported
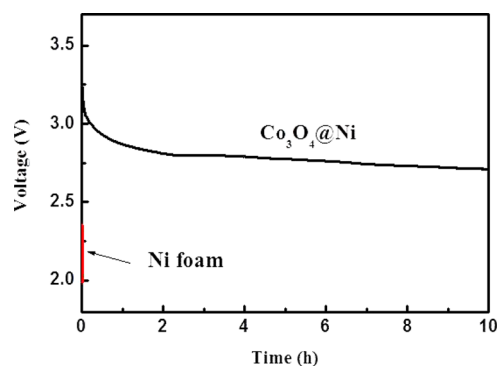

Figure 4. Comparable discharge curves of pure nickel foam and the Co$_3$O$_4$@Ni electrode in O$_2$ at a current density of 0.05 mA cm^{-2} (the discharge time for Co$_3$O$_4$@Ni electrode is ∼72 h).

carbon-based electrodes catalyzed by cobalt oxides (compared to ∼4.0 V of Co$_3$O$_4$/Super P, 4.12 V of CoO$_x$/DLC, and 4.0 V of CoO/CMK-3).[13,28,29] It implies the synergistic catalytic effect of Co$_3$O$_4$ in the Co$_3$O$_4$@Ni architectural structure for the oxygen evolution reaction. Figure 3b presents the initial charge/discharge profiles for the lithium−oxygen batteries at different current densities. When the applied current density increases to 0.2 mA cm^{-2}, the battery exhibits a discharge capacity of 577 mAh g^{-1}, which decreases to 212 mAh g^{-1} at 0.5 mA cm^{-2}. The fast capacity decay is accompanied by a significant increase in the polarization, mainly attributed to the rise in the electrode resistance and oxygen diffusion limit.

The full charge/discharge cycling performance of the battery was investigated at a current density of 0.2 mA cm^{-2}. It could be detected from Figure 5c that dramatic capacity fading is observed from the second cycle and a discharge capacity valley of 326 mAh g^{-1} was obtained at 8th cycle. The charge/discharge processes of the initial several cycles promote good contact between the electrolyte and the active material. The triphase reaction takes place at the inner pores, resulting in a small rebound in the discharge capacity. However, the capacity decreases gradually to 231 mAh g^{-1} at 100th cycle. It should be noted that nonaqueous lithium−oxygen batteries generally exhibit poor cycling performance at full charge/discharge condition. This is because the full charge/discharge processes aggravate the byproducts accumulation and thus passivate the air electrode. Besides, it is reported in a previous investigation that the continuous gas/solid conversion provokes volume change in the air electrode.[30] During the full charge/discharge cycles, the volume change lessens the compact contact between the active material and limit the cycling performance. Moreover, as an open system, the gradual loss of electrolyte caused by the longtime operation also deteriorates the degradation.[31]

The impedance variation of the lithium−oxygen battery was monitored by electrochemical impedance spectroscopy (EIS) to check the charge efficiency of the air electrode. As shown in Figure 5d, the charge transfer resistance increases after discharge, which could be due to the generation of the insulating discharge products. It becomes smaller when the battery is charged, but still slightly larger than that before discharging. There are two possible factors to affect the increased impendence: (1) the incomplete decomposition of byproduct, induced by the potential reaction between Li$_2$O$_2$ and the electrolyte solvent; (2) the formation/decomposition
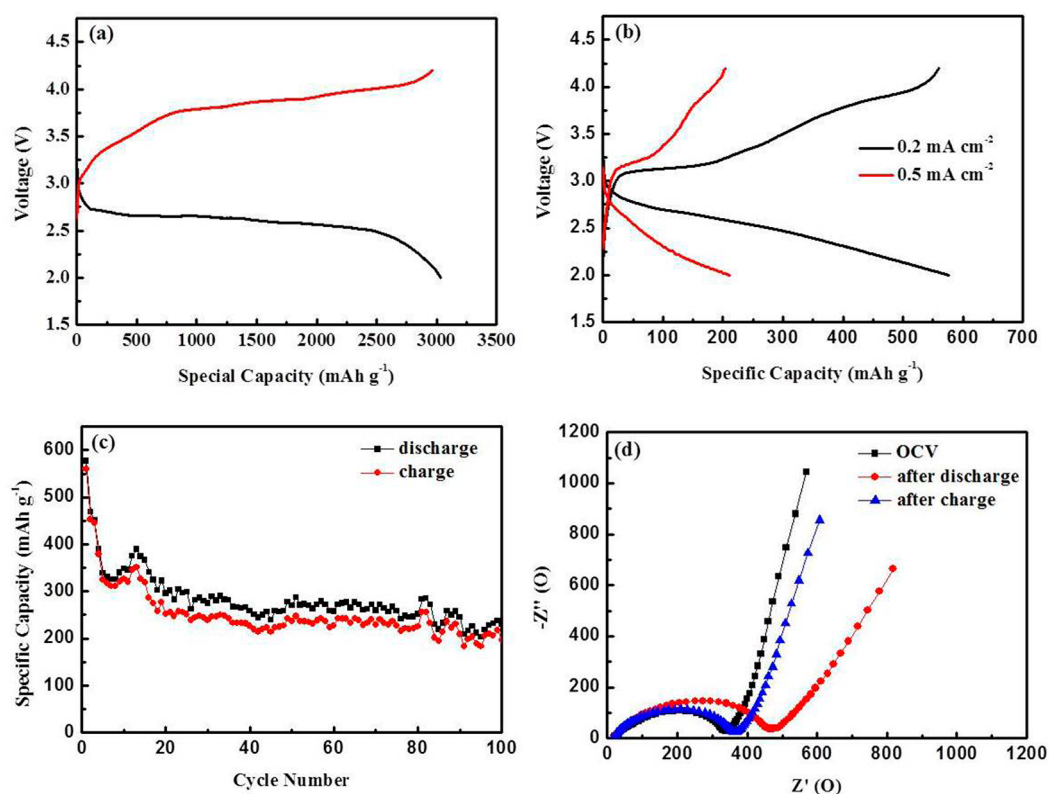
Figure 5. Charge/discharge curves of the Co₃O₄@Ni electrode tested at (a) a current density of 0.05 mA cm⁻² and (b) different current densities. (c) Cycling performance of the Co₃O₄@Ni electrode at 0.2 mA cm⁻². (d) Electrochemical impedance spectra of the Co₃O₄@Ni electrode in the first cycle.
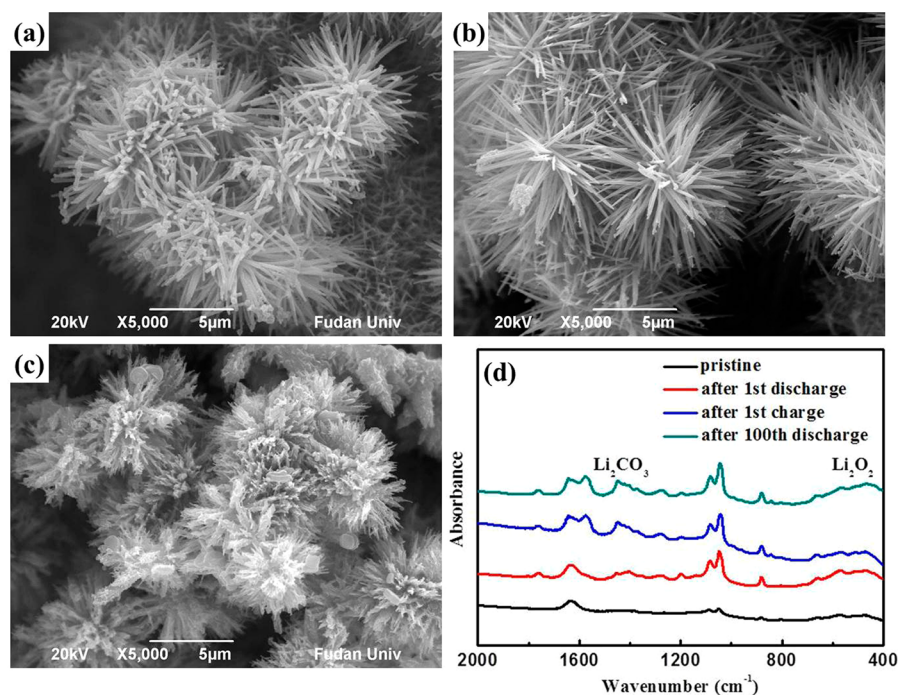

Figure 6. SEM images of the Co₃O₄@Ni electrode (a) after 1st discharge, (b) after 1st charge, and (c) after the 100th cycle. (d) FTIR spectra of the Co₃O₄@Ni electrode at the end of discharge and charge.

of Li_2O_2 particles lessens the compact contact between Co_3O_4 microspheres.

To clarify the corresponding relationship between the achieved performance of the Co₃O₄@Ni-based battery and

the unique hierarchical porous structure, the morphologies of the electrode at different stages were analyzed by ex situ SEM technology. The SEM image of the fully discharged electrode demonstrates that the discharged products are growing along
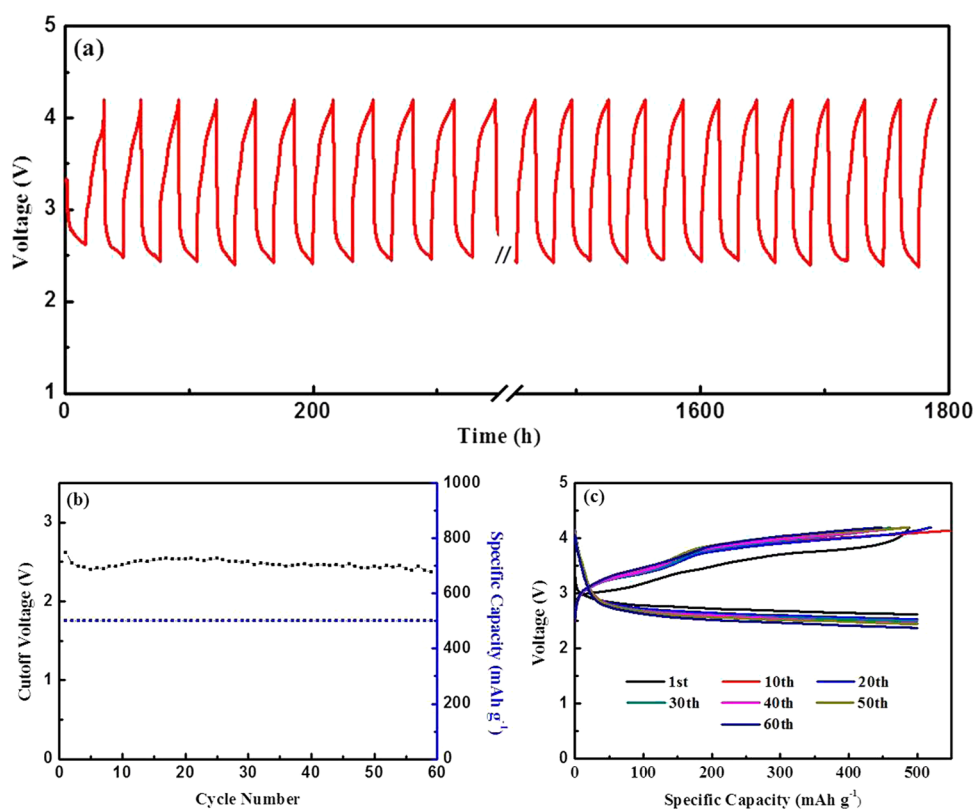
Figure 7. (a) Cycling performance, (b) the plots of cutoff voltage vs cycle number, and (c) the discharge/charge profiles at various cycles of the $Co_3O_4@Ni$ electrode with a restriction of the capacity of 500 mAh g^{-1} at a current density of 0.05 mA cm^{-2}.

the 1D nanorods and partly occupy the void spaces between the nanorods. However, no blockage or clogging is observed, even during the deep discharge state. This result indicates the macrosized void spaces in the electrode proved efficient accommodation places for Li_2O_2 deposition. After charge, Li_2O_2 disappears and the surface of the 1D nanorods becomes as smooth as those in Figure 1d−f, implying the decomposition of the discharge product and the reversibility of the electrode, which is in accord with the results of EIS. Additional SEM imaging of the electrode after 100 cycles shows that Li_2O_2 deposition fills the pores built up by the 1D nanorods. It is noteworthy that the open framework of the air electrode is well maintained even after 100 cycles. However, the SEM investigation is not enough to clarify the reversibility of the batteries, and then FTIR was further introduced to demonstrate the reversible conversation between O_2 and Li_2O_2 over charge/discharge processes. It can be observed from Figure 6d that the characteristic peaks assigned to Li_2O_2 appear at the end of discharge and vanish again in the spectrum after the charge process. However, the peaks in addition to Li_2O_2 may be associated with the Li_2CO_3 contributed by the undesired decomposition of electrolyte. In view of the FTIR results, it can be concluded that Li_2O_2 deposition becomes dominant after the 1st discharge, but the presence of the slight TEGDME decomposition cannot be ignored, which is consistent with previous reports.[32−35] However, the peaks related to Li_2CO_3 become apparent after the 100th cycle, indicating the continuous accumulation of undesired products and aggravating the polarization of the air electrode.

However, a deep discharge to 2 V substantially increases the resistance of the electrode, and causes severe polarization. In order to avoid large voltage polarization to some extent, a

restriction should be put to the depth of discharge. Herein we also tested the cycling performance of the $Co_3O_4@Ni$ electrode at a current density of 0.05 mA cm^{-2} with a limited capacity of 500 mAh g^{-1}. As listed in Figure 7, the $Co_3O_4@Ni$-based battery could be discharged and charged between 2.0 and 4.2 V vs Li/Li^+ for 60 cycles (~1800 h), where the cutoff voltage remains above 2.45 V. No significant change in the discharge/charge profiles is observed during cycling. However, the Coulombic efficiency exceeds over 100% at some cycles, which indicates that the undesired electrolyte decomposition is accompanied during the charge process. The encouraging cycling performance of the $Co_3O_4@Ni$ electrode could be ascribed to its unique architecture: (1) the open structure facilitates electrolyte penetration and the ion/electron transfer; (2) the macrosized voids between the nanorods provide sufficient buffer space for Li_2O_2 deposition without blocking O_2 diffusion.

■ CONCLUSIONS

In summary, a facile method was used to grow sea-urchin-like Co_3O_4 on nickel foam, and the resulting composite was applied as the carbon-free electrode in the lithium−oxygen batteries. It is demonstrated that the unique hierarchical structure plays an active role in improving the electrochemical performance. The $Co_3O_4@Ni$ electrode delivers not only high capacity but also long cycle life (~1800 h, 60 cycles) at a limit capacity of 500 mAh $g^{-1}_{electrode}$. The encouraging performance can be ascribed to the favorable ion/electron transfer, the adequate buffer space for Li_2O_2 deposition/decomposition and the facilitated O_2 diffusion from macrosized void spaces. This work may provoke some thinking on the design of more advanced electrode architectures, though the electrolyte choice is still challenge for

the construction of rechargeable nonaqueous lithium−oxygen batteries.

■ AUTHOR INFORMATION

Corresponding Author

*A. Yu. Tel.: +86-21-51630320. Fax: +86-21-51630320. E-mail address: asyu@fudan.edu.cn.

Notes

The authors declare no competing financial interest.

■ REFERENCES

(1) Abramham, K.; Jiang, Z. A polymer electrolyte-based rechargeable lithium/oxygen battery. *J. Electrochem. Soc.* **1996**, *143*, 1−5.

(2) Girishkumar, G.; McCloskey, B.; Luntz, A. C.; Swanson, S.; Wilcke, W. Lithium−air battery: Promise and challenges. *J. Phys. Chem. Lett.* **2010**, *1*, 2193−2203.

(3) Zhang, S. S.; Foster, D.; Read, J. Discharge characteristic of a non-aqueous electrolyte Li/O$_2$ battery. *J. Power Sources* **2010**, *195*, 1235−1240.

(4) Yoo, E.; Zhou, H. S. Li−air rechargeable battery based on metal-free graphene nanosheet Catalysts. *ACS Nano* **2011**, *5*, 3020−3026.

(5) Xiao, J.; Mei, D. H.; Li, X. L.; Xu, W.; Wang, D. Y.; Graff, G. L.; Bennett, W. D.; Nie, Z. M.; Saraf, L. V.; Aksay, I. A.; Liu, J.; Zhang, J. G. Hierarchically porous graphene as a lithium−air battery electrode. *Nano Lett.* **2011**, *11*, 5071−5078.

(6) Mirzaeian, M.; Hall, P. J. Preparation of controlled porosity carbon aerogels for energy storage in rechargeable lithium oxygen batteries. *Electrochim. Acta* **2009**, *54*, 7444−7451.

(7) Beattie, S. D.; Manolescu, D. M.; Blair, S. L. High-capacity lithium−air cathodes. *J. Electrochem. Soc.* **2009**, *156*, A44−A47.

(8) Xiao, J.; Wang, D. H.; Xu, W.; Wang, D. Y.; Williford, R. E.; Liu, J.; Zhang, J. G. Optimization of air electrode for Li/air batteries. *J. Electrochem. Soc.* **2010**, *157*, A487−A492.

(9) Li, Y. L.; Wang, J. J.; Li, X. F.; Geng, D. S.; Yang, J. L.; Li, R. Y.; Sun, X. L. Nitrogen-doped carbon nanotubes as cathode for lithium−air batteries. *Electrochem. Commun.* **2011**, *13*, 668−672.

(10) Li, Y. L.; Wang, J. J.; Li, X. F.; Geng, D. S.; Li, R. Y.; Sun, X. L. Superior energy capacity of graphene nanosheets for a nonaqueous lithium-oxygen battery. *Chem. Commun.* **2011**, *47*, 9438−9440.

(11) Sun, B.; Wang, B.; Su, D. W.; Xiao, L.; Ahn, H.; Wang, G. X. Graphene nanosheets as cathode catalysts for lithium-air batteries with an enhanced electrochemical performance. *Carbon* **2012**, *50*, 727−733.

(12) Black, R.; Oh, S. H.; Lee, J. H.; Yim, T.; Adams, B.; Nazar, L. F. Screening for superoxide reactivity in Li-O$_2$ batteries: Effect on Li$_2$O$_2$/LiOH crystallization. *J. Am. Chem. Soc.* **2012**, *134*, 2902−2905.

(13) Débart, A.; Bao, J. L.; Armstrong, G.; Bruce, P. G. An O$_2$ cathode for rechargeable lithium batteries: The effect of a catalyst. *J. Power Sources* **2007**, *174*, 1177−1182.

(14) Débart, A.; Paterson, A. J.; Bao, J. L.; Bruce, P. G. α-MnO$_2$ nanowires: A catalyst for the O$_2$ electrode in rechargeable lithium batteries. *Angew. Chem., Int. Ed.* **2008**, *47*, 4521−4524.

(15) Lu, Y. C.; Xu, Z. C.; Gasteiger, H. A.; Chen, S.; Kimberly, H. S.; Yang, S. H. Platinum−gold nanoparticles: A highly active bifunctional electrocatalyst for rechargeable lithium−air batteries. *J. Am. Chem. Soc.* **2010**, *132*, 12170−12171.

(16) McCloskey, B. D.; Speidel, A.; Scheffler, R.; Miller, D. C.; Viswanathan, V.; Hummelshoj, J. S.; Norskov, J. K.; Luntz, A. C. Twin problems of interfacial carbonate formation in nonaqueous Li−O$_2$ batteries. *J. Phys. Chem. Lett.* **2012**, *3*, 997−1001.

(17) McCloskey, B. D.; Bethune, D. S.; Shelby, R. M.; Mori, T.; Scheffler, R.; Speidel, A.; Sherwood, M.; Luntz, A. C. Limitations in rechargeability of Li-O$_2$ batteries and possible origins. *J. Phys. Chem. Lett.* **2012**, *3*, 3043−3047.

(18) Li, F. J.; Zhang, T.; Zhou, H. S. Challenges of non-aqueous Li−O$_2$ batteries: Electrolytes, catalysts, and anodes. *Energy Environ. Sci.* **2013**, *6*, 1125−1141.

(19) Peng, Z. Q.; Freunberger, S. A.; Chen, Y. H.; Bruce, P. G. A reversible and higher-rate Li-O$_2$ battery. *Science* **2012**, *337*, 563−566.

(20) Li, F. J.; Tang, D. M.; Chen, Y.; Golberg, D.; Kitaura, H.; Zhang, T.; Yamada, A.; Zhou, H. S. Ru/ITO: A carbon-free cathode for nonaqueous Li−O$_2$ battery. *Nano Lett.* **2013**, *13*, 4702−4707.

(21) Li, F. J.; Tang, D. M.; Jian, Z. L.; Liu, D. Q.; Golberg, D.; Yamada, A.; Zhou, H. S. Li-O$_2$ battery based on highly efficient Sb-doped tin oxide supported Ru nanoparticles. *Adv. Mater.* **2014**, *26*, 4659−4664.

(22) Riaz, A.; Jung, K. N.; Chang, W. Y.; Lee, S. B.; Lim, T. H.; Park, S. J.; Song, R. H.; Yoon, S.; Shin, K. H.; Lee, J. W. Carbon-free cobalt oxide cathodes with tunable nanoarchitectures for rechargeable lithium−oxygen batteries. *Chem. Commun.* **2013**, *49*, 5984−5986.

(23) Zhao, G. Y.; Xu, Z. M.; Sun, K. N. Hierarchical porous Co$_3$O$_4$ films as cathode catalysts of rechargeable Li-O$_2$ batteries. *J. Mater. Chem. A* **2013**, *1*, 12862−12867.

(24) Lee, H.; Kim, Y. J.; Lee, D. J.; Song, J. C.; Lee, Y. M.; Kim, H. T.; Park, J. K. Directly grown Co$_3$O$_4$ nanowire arrays on Ni-foam: Structural effects of carbon-free and binder-free cathodes for lithium-oxygen batteries. *J. Mater. Chem. A* **2014**, *2*, 11891−11898.

(25) Zhao, Y. L.; Xu, L.; Mai, L. Q.; Han, C. H.; An, Q. Y.; Xu, X.; Liu, X.; Zhang, Q. J. Hierarchical mesoporous perovskite La$_{0.5}$Sr$_{0.5}$CoO$_{2.91}$ nanowires with ultrahigh capacity for Li-air batteries. *Proc. Natl. Acad. Sci. U. S. A.* **2012**, *109*, 19569−19574.

(26) Laoire, C. O.; Mukerjee, S.; Abraham, K. M.; Phichta, E. J.; Hendrickson, M. A. Influence of nonaqueous solvents on the electrochemistry of oxygen in the rechargeable lithium-air battery. *J. Phys. Chem. C* **2010**, *114*, 9178−9186.

(27) Lu, Y. C.; Ynag, S. H. Probing the reaction kinetics of the charge reactions of nonaqueous Li−O$_2$ batteries. *J. Phys. Chem. Lett.* **2013**, *4*, 93−99.

(28) Sun, B.; Liu, H.; Munroo, P.; Ahn, H.; Wang, G. X. Nanocomposites of CoO and a mesoporous carbon (CMK-3) as a high performance cathode catalyst for lithium-oxygen batteries. *Nano Res.* **2012**, *5*, 460−469.

(29) Yang, Y.; Sun, Q.; Li, Y. S.; Li, H.; Fu, Z. W. A CoOx/carbon double-layer thin film air electrode for nonaqueous Li-air batteries. *J. Power Sources* **2013**, *223*, 312−318.

(30) Yoo, K.; Soumik, B.; Dutta, P. Modeling of volume change phenomena in a Li−air battery. *J. Power Sources* **2014**, *258*, 340−350.

(31) Wu, G.; Mack, N. H.; Gao, W.; Mao, S.; Zhong, R.; Han, J.; Baldwin, J. K.; Zelenay, P. Nitrogen-doped graphene-rich catalysts derived from heteroatom polymers for oxygen reduction in nonaqueous lithium−O$_2$ battery cathodes. *ACS Nano* **2012**, *6*, 9764−9776.

(32) McCloskey, B. D.; Bethune, D. S.; Shelby, R. M.; Girishkumar, G.; Luntz, A. C. Solvents' critical role in nonaqueous lithium−oxygen battery electrochemistry. *J. Phys. Chem. Lett.* **2011**, *2*, 1161−1166.

(33) Xu, J. J.; Wang, Z. L.; Xu, D.; Zhang, L. L.; Zhang, X. B. Tailoring deposition and morphology of discharge products towards high-rate and long-life lithium-oxygen batteries. *Nat. Commun.* **2013**, *4*, 2438−2448.

(34) Thotiyl, M. M. O.; Freunberger, S. A.; Peng, Z. Q.; Chen, Y. H.; Liu, Z.; Bruce, P. G. A stable cathode for the aprotic Li-O$_2$ battery. *Nat. Mater.* **2013**, *12*, 1050−1056.

(35) Balaish, M.; Kraysberg, A.; Ein-Eli, Y. A critical review on lithium−air battery electrolytes. *Phys. Chem. Chem. Phys.* **2014**, *16*, 2801−2822.